A simple boundary-layer transition detection method using mean static pressure measurements

Jenna Eppink[1] · Judith Hannon[1] · Andrew Leidy[1] · Michael Kegerise[1]

Received: 21 November 2022 / Revised: 15 February 2023 / Accepted: 28 March 2023

Abstract

A simple method for detecting boundary-layer transition using only mean static pressure port data is presented. The method can be applied to many existing models with pressure taps and only requires that a fine angle of attack sweep be performed. A small but abrupt change in the static pressure is visible when the transition front passes over the pressure tap. Results from a recent Juncture Flow test entry are used to illustrate the technique. Infrared thermography measurements of the transition front compare very well to the transition locations obtained from the static pressure ports. Some differences in behavior occur depending on the dominant transition mechanism. While the technique is somewhat qualitative, it can be an excellent tool for estimating the transition location when other tools are not readily available. Given the simplicity of the technique, and the fact that many wind-tunnel models are already designed with numerous static pressure taps, this method can be applied with very little overhead.

Graphical abstract

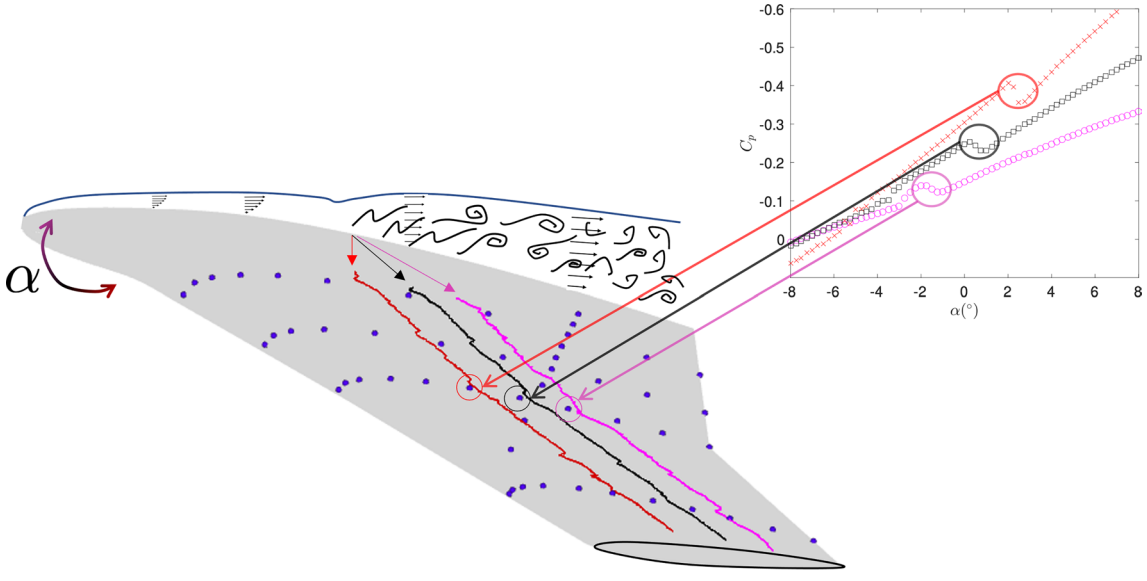

Judith Hannon, Andrew Leidy, and Michael Kegerise have contributed equally to this work.

✉ Jenna Eppink
jenna.eppink@nasa.gov

Judith Hannon
judith.a.hannon@nasa.gov

Andrew Leidy
andrew.leidy@nasa.gov

Michael Kegerise
michael.a.kegerise@nasa.gov

[1] Flow Physics and Control Branch, NASA Langley Research Center, Hampton, VA 23681, USA

1 Introduction

Boundary-layer transition is an important flow phenomenon that can have significant impacts on the performance of a wind-tunnel model. However, transition measurements can be challenging to acquire. Optical-based techniques are often used, but these require optical access to the surface of the model, and, depending on the technique, special cameras, windows, coatings on the model, etc. One common example is infrared (IR) thermography, which relies on the fact that the convective heating in a turbulent boundary layer differs from that in a laminar boundary layer, and the resulting temperature difference should be visible in an IR image (Quast 1987). Alternatively, surface-mounted high-speed pressure (Huang and Hannan 1975) or hot-film sensors (Liepmann and Skinner 1954) can be utilized, but these are often expensive and require additional instrumentation, and therefore will be located only in very limited regions of the model.

On the other hand, wind-tunnel testing routinely includes measurements of static pressures along the model surface. These pressure measurements are much cheaper to acquire than, for instance, high-speed pressure measurements. Due to their already widespread use, if it were possible to utilize these static pressure sensors to detect boundary-layer transition, this could provide a valuable tool for acquiring transition data in tests where it may otherwise not be feasible to do so. One such approach was proposed by Gardner and Richter (2015), who used unsteady Kulite pressure transducers embedded in the static pressure taps of the model to obtain the fluctuating signal. They found that it was possible to identify the transition location based on the root-mean-square (RMS) of the fluctuating signal. They also were able to use the standard deviation of the signal, low-pass filtered at 1 Hz, to detect transition. Thus, it is likely possible to apply this approach using the standard electronically scanned pressure (ESP) setup, avoiding the use of expensive high-speed pressure transducers, though it has not been directly demonstrated.

In theory, it is possible to locate the transition front simply by viewing a traditional mean static pressure distribution. This fact was exploited by Popov et al. (2008), who used the slope of computed pressure coefficient (C_p) distributions to estimate the transition location on an airfoil. They observed that there is a slight, but abrupt, rise in pressure at the transition location. While they attributed this phenomenon to the existence of a separation bubble in the boundary layer, it actually occurs even when a separation bubble is not present, which will be demonstrated in this letter. The pressure rise is likely caused by the rapid change in the growth of the boundary layer at or near the transition location, resulting in a rather abrupt change in the displacement thickness. This effect can be seen in numerous computational results (see Venkatachari et al. (2021), for example), but is often dismissed as a computational artifact. However, this abrupt pressure rise is actually a physically present phenomenon. Unfortunately, one would be unlikely to observe this phenomenon in a typical experimental setup because of the spatial resolution that would be required to see such a small and localized rise in pressure. On the other hand, the transition location is usually expected to move slowly along the surface as the angle of attack is changed. Thus, with small enough increments in the angle of attack, one should be able to observe the passage of the transition front over a static pressure tap. This approach forms the basis of the method that will be described and demonstrated in this letter.

2 Experimental methods

2.1 Juncture flow experiment

The NASA Juncture Flow Experiment was designed to critically assess and improve upon existing turbulence models using validation-quality flow-field data acquired in the wing-fuselage junction region. The full-span wing-fuselage model has been tested three times in the NASA Langley 14- by 22-Foot Subsonic Tunnel. The third phase of testing, from which data are presented in this paper, was performed using a symmetric profile swept wing (Leidy et al. 2023). The semi-span (b) of the symmetric wing was 1.6635 m, with a leading edge sweep of approximately 37.3° and a crank chord, c, of 581 mm. The entire configuration was top-bottom symmetric. Testing was performed at a fixed crank-chord-based Reynolds (Re) number of 2.4 million, with angles of attack (α) ranging from −10° to + 10°. Since the 14×22 is not a temperature-controlled facility, the temperature drift resulted in a range of Mach numbers from approximately 0.175 to 0.205.

The wings were instrumented with 266 static pressure ports. The port wing contained 7 streamwise rows of pressure taps, while the starboard wing contained 5, located at the same spanwise and streamwise positions as the 5 outboard rows on the port wing. The pressure taps along each row were aligned in the streamwise direction (i.e., on the same butt line). The inner diameter of each pressure port was 597–648 μm. ESP modules were used to measure the mean pressure at each port. The full-scale range of the modules was 6.89 kPa (1 psid) or 34.47 kPa (5 psid) depending on the expected pressure range of the ports connected to the module, and the modules were referenced to the ambient pressure in the control room of the wind-tunnel facility. Based on the accuracy of the modules and the tunnel calibration

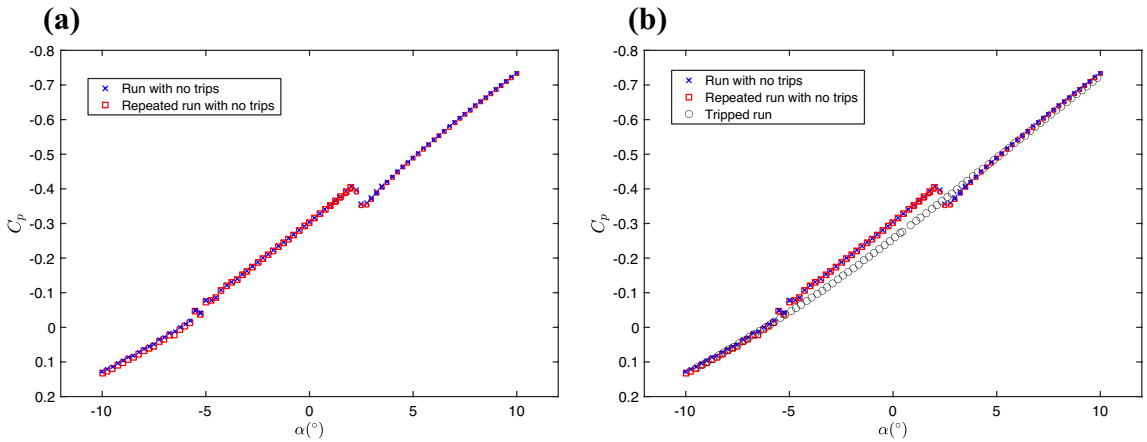

Fig. 1 C_p versus α for the fine alpha sweep runs for the pressure tap located at $x/c = 0.35$, $y/b = 0.523$ mm on the port wing. **a** Only the natural transition runs and **b** including the tripped run

uncertainty, the estimated uncertainty for the two modules in terms of C_p corresponds to 0.002–0.004 and 0.006–0.008, respectively. More details of the Juncture Flow experiment can be found in Leidy et al. (2023), Rumsey et al. (2022), Venkatachari et al. (2021), and Rumsey (2022).

The third phase of testing included IR thermography measurements of the upper wing surface in order to measure the transition front at various angles of attack. Thus, for some portions of the testing, no boundary-layer tripping was performed to allow the natural transition process to occur. When a turbulent boundary layer was desired over the entire wing surface, trip-dot arrays were used to fix the transition location. The trip dots were applied near the leading edge of the wings with a commercially-produced trip-dot tape that is available in a range of heights.

2.2 Data processing methods

2.2.1 IR image acquisition and transition front processing

The top surface of each wing was viewed by separate IR cameras looking through two different open ports in the ceiling. IR images were acquired once the tunnel was on condition, and the model reached the desired angle of incidence. One hundred frames were taken at each point, with a typical exposure time of 15 ms, which was chosen to maximize the dynamic range of the 14-bit detector. For processing, the one hundred frames were averaged, and any noisy pixels were filtered through outlier detection. The distortion was removed from the images using the camera calibration. A surface mesh was then generated for each image, with streamwise (x) resolution between 1 and 2 mm depending on the angle of incidence and spanwise (y) resolution of 0.5 mm. The intensity values, I, were then projected onto the mesh points. The intensity values along each streamwise slice (i.e., constant y) were evaluated in terms of streamwise distance (x). The derivative of the curve ($\partial I/\partial x$) was approximated using a central difference scheme. The maximum values of the derivatives at each spanwise location were used to determine the transition front location, utilizing the surrounding transition location estimates to filter out any spurious values. More details regarding the IR acquisition and processing approach can be found in Leidy et al. (2023). For a comparison of the IR transition detection technique against hot films (a more traditional method), the reader is referred to Hall et al. (1989).

2.2.2 Transition detection technique using static pressures

As described in Sect. 1, a slight rise in the surface static pressure occurs locally at the boundary-layer transition location. As will be the case for most models, the streamwise spacing of the pressure taps in the current experiment is too sparse to enable observation of the pressure rise directly from a plot of C_p versus x. Even if the streamwise spacing were fine enough, the variability between different pressure taps in the form of bias could potentially make it difficult to observe such a small change in pressure. However, when an angle of attack sweep is performed with a small enough step in α, the pressure rise at a given pressure tap is quite noticeable when the C_p values are plotted against angle of attack. The required α-step size is probably not easy to predict, as it will likely be dependent on the flow conditions (specifically Re), the dominant transition mechanism, and the resolution of the ESP module used for the measurement. For this experiment, a step size of 0.25° in α was chosen to demonstrate this technique.

Example results from one pressure port are shown in Fig. 1. Figure 1a includes only the natural transition runs,

while Fig. 1b includes a tripped (fully turbulent) run for comparison. Note that there are actually two points of transition occurring in this figure. At the most negative angles of attack, the flow at this location (corresponding to $x/c = 0.35$) is already turbulent. As the angle of attack is increased, the flow becomes laminar, since the transition front is moving downstream. This results in a slight decrease in pressure at $\alpha \approx -5°$. As the angle of attack is further increased, the transition front moves upstream once again. This is due to a change in the dominant transition mechanism from stationary crossflow (SCF) instabilities to Tollmien–Schlichting (TS) waves (Venkatachari et al. 2021). Once again, the flow becomes turbulent at this pressure port at $\alpha \approx 2°$. Note that the abrupt changes in pressure are extremely repeatable, as two completely independent runs are being compared in Fig. 1a.

For the results presented later in this letter, the transition location was identified as the central portion of the "kink" in the C_p versus α plot for each pressure tap. It should be noted that this technique is, by nature, somewhat qualitative, as it requires a manual visual identification of the abrupt pressure change in the C_p versus α plot. It may be possible to develop an automated approach to extract the transition locations; however, this approach would still likely vary depending on the configuration. If the test allows, and as long as the C_p measurements are repeatable from run to run, a more quantitative way of assessing the results is to compare to a fully turbulent (i.e., tripped) configuration. For the current test, tripped runs were performed; thus, direct comparisons can be made, such as in Fig. 1b. The departure of the C_p values of the untripped configurations from the tripped C_p values provides an even clearer indication of the angles at which the sensor is under a laminar or a turbulent boundary layer.

3 Results

Similar to Fig. 1, the C_p results are plotted versus angle of attack for each pressure port, and the transition α is extracted from each plot. At some pressure tap locations, as shown in Fig. 1, there are actually two points of transition, and these are identified as either TS- or SCF-dominated transition. The dominant transition mechanism can be inferred from multiple sources. The IR images from the current test verify a more jagged transition front on the upper surface of the wing at the larger negative angles of attack, implying that SCF instabilities are the dominant transition mechanism, while the transition front appears smooth at positive angles of attack, implying TS-dominated transition. These observations are confirmed by the pre-test computations performed by Venkatachari et al. (2021).

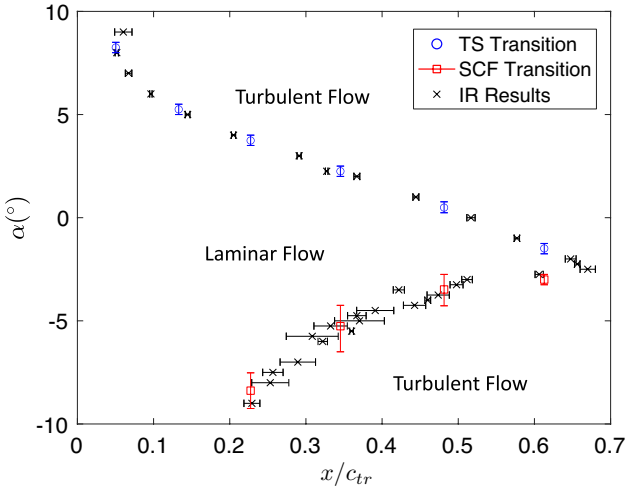

Fig. 2 Transition locations (x/c_{tr}) versus angle of attack for the pressure port row located at $y/b = 0.523$ on the port wing. Vertical error bars correspond to the α-range over which the kink occurs in the C_p versus α curve. Horizontal error bars for the IR data represent the RMS uncertainty associated with the random uncertainty (run-to-run variability) and the systematic uncertainty (due to photogrammetric projection errors)

Combined results for the row of pressure taps at $y/b = 0.523$ on the port wing of the model are shown in Fig. 2. The transition locations inferred from the C_p versus α plots of all pressure taps along that streamwise row are plotted as the red and blue symbols. While this row actually contained 11 pressure taps along the top surface, only the ones that showed the passage of the transition front are included in this plot. Visualizing the data in this way allows us to verify that the kinks in the C_p versus α plots are indeed indicative of transition, as the transition front movement behaves as expected. Due to the qualitative nature of this approach, error bars are included in this plot to illustrate the potential variability involved in identifying the kink location. The variability is clearly much larger for the cases where SCF is dominant. Additionally, the transition locations obtained from the IR images are included in this figure, along with their estimated uncertainties, to compare directly with the C_p results. The transition results obtained from both methods compare very well, indicating that this method of extracting transition location directly from pressure data is a valid approach. Notice, however, that at the more negative angles of attack, when transition is dominated by SCF instabilities, the transition front does not monotonically or smoothly move downstream, as indicated clearly by the IR results. This is in agreement with the seemingly erratic, but repeatable, behavior observed in Fig. 1 near $\alpha = -5°$. Unfortunately, this behavior can make it difficult to extract the transition location from the C_p versus α plot in some instances, since there is not a clear localized "kink" in the distribution. The larger error bars in the C_p-derived

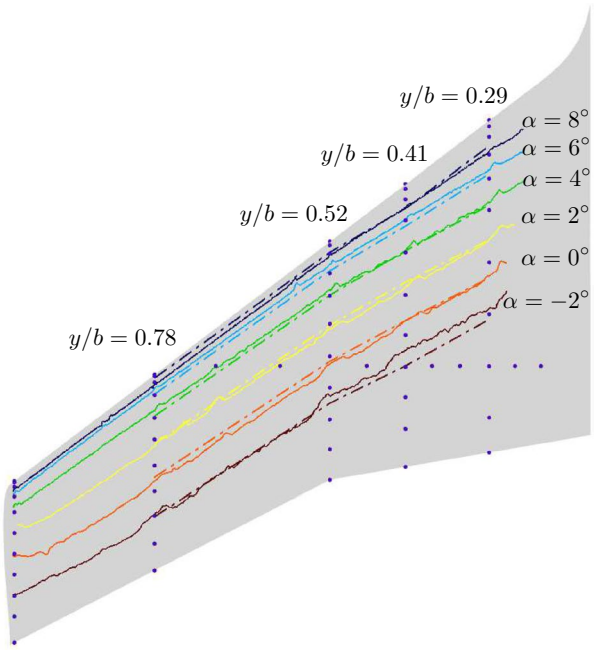

Fig. 3 Comparison of the IR transition fronts (solid lines) with the transition fronts estimated from the pressure ports (dashed lines) for various angles of attack on the port wing

measurement locations for the SCF-dominated transition cases illustrate this increased level of variability. There is also significantly more uncertainty in the IR measurements for these cases as well. Overall, the differences seen in this plot fall within the range of estimated uncertainties, and the results obtained from this row of pressure taps agree very well with the transition front obtained from the IR images for both the SCF- and TS-dominated transition regimes.

Finally, the transition fronts obtained from the two different methods are compared at multiple spanwise locations. These results are compiled for the port wing in Fig. 3 for the range of $\alpha = -2°$ to 8°. To directly compare the results for a given angle of attack, it was necessary to interpolate the α versus x/c_{tr} curve (such as those shown in Fig. 2) to obtain the transition location for each spanwise row. A quadratic fit was applied to each curve and interpolated for the desired α. For the data shown in Fig. 3, the RMS difference between the two methods was 13.75 mm, corresponding to $\Delta x/c \approx 0.024$, and the largest difference was 37 mm, or $\Delta x/c \approx 0.06$, occurring near the inboard trailing edge of the wing at $\alpha = -2°$. The agreement between the two methods is quite good, especially considering the limited spatial resolution of the pressure measurements.

In order to demonstrate the importance of the fine α -resolution, results are presented at two pressure taps along the $y/b = 0.523$ row. In Fig. 4a, the original α-resolution of 0.25° is used. In Fig. 4b, the data are downsampled (every fourth point is kept) to illustrate the results that would have been obtained with an α-resolution of 1°. For the pressure tap at $x/c = 0.133$, a kink is clearly visible near $\alpha = 5°$ in the original data, but it is no longer visible in the downsampled data. However, at $x/c = 0.345$, the kink near $\alpha = 3°$ is large enough that it is visible in both plots. On the other hand, the smaller kinks that occur due to the SCF-dominated transition near $\alpha = -5°$ are very difficult to distinguish in the downsampled plot. These results illustrate that the α-resolution that is required to clearly resolve the transition location is strongly case dependent. Thus, for the best chance of success, data should be acquired with the smallest possible α resolution.

Figures 4c and d are included to briefly illustrate the possibility of using the unsteady C_p data in conjunction with the mean kink approach. For each mean C_p value, 80 points were acquired at 10 Hz, from which we can also compute a standard deviation (σ_{C_p}). At the most upstream pressure port, $x/c = 0.133$, the σ_{C_p} results are inconclusive, as there is no clear peak evident. However, at $x/c = 0.345$, there are large peaks in σ_{C_p} when the transition front passes over the pressure port. The peak near $\alpha = -5°$ corresponding to SCF-dominated transition is quite a bit broader, likely due to the non-monotonic nature of the transition front movement. Because this peak is broader, it is maintained in the downsampled data, while the peak due to TS transition near $\alpha = 3°$ is no longer visible. In the current dataset, we have found that for the TS-dominated transition cases, the σ_{C_p} -approach is less reliable than using the mean kink analysis for obtaining the transition location. However, when SCF is dominant, since the kinks in the mean C_p are often less clearly defined, the σ_{C_p}-approach makes it easier to identify the transition location in those cases, and it certainly provides an extra level of confidence in the results.

4 Conclusions

A simple, yet powerful, technique for determining the boundary-layer transition location using static pressure taps was presented. The method exploits the fact that an abrupt increase in surface static pressure occurs on the model at the transition location. The basic approach is to perform a fine sweep over the angle of attack range of interest and then plot the C_p versus α data for each pressure tap. The transition point is then identified as the angle of attack at which the abrupt increase in static pressure occurs. As this method simply requires a small change in transition front location with each step in α, a potential variation of this approach would be to do a fine Reynolds number sweep at a fixed α, though this approach has not yet been tested.

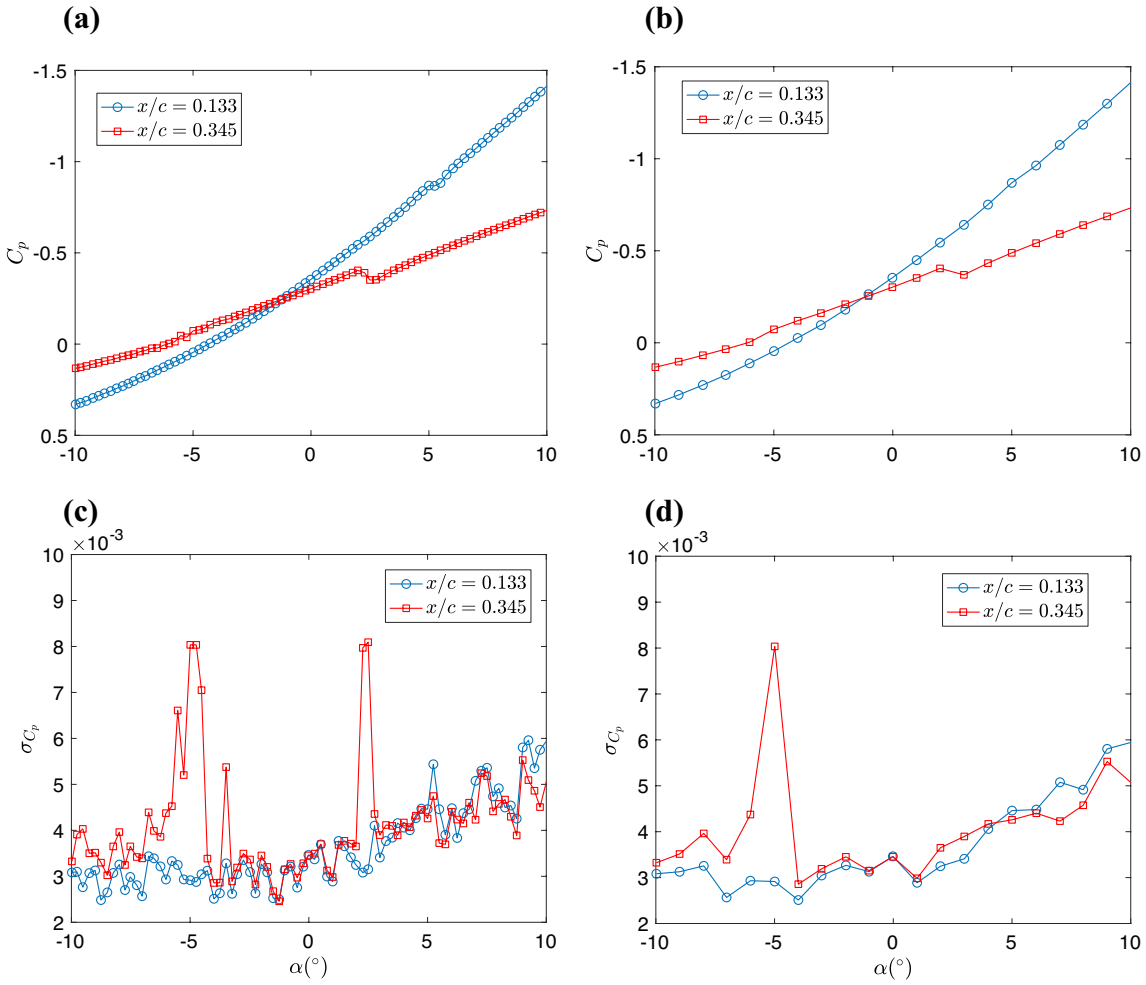

Fig. 4 C_p and standard deviation (σ_{C_p}) results for two different pressure ports along the $y/b = 0.523$ row, with **a**, **c** $\Delta\alpha = 0.25°$ and **b**, **d** down-sampled to obtain $\Delta\alpha = 1°$

Given the prevalence of static pressure measurements on wind-tunnel models, this technique could prove to be a valuable tool. The only potential added cost is the extra time required to do the fine angle of attack sweeps, but the required α-resolution will probably be case dependent. In fact, it is very likely that numerous wind-tunnel datasets already exist that would benefit from the application of this technique. In some cases, it also may be necessary to consider the resolution of the ESP module that will be used for a test, as the C_p measurement resolution could impact the effectiveness of this technique. While it may be beneficial to include tripped boundary-layer runs in the test matrix to compare with natural transition, as shown in this letter, it is not a requirement. Another potential application for this technique is to verify the effectiveness of different tripping configurations, particularly in cases where no other methods are available for measuring transition. It was also demonstrated that the technique proposed by Gardner and Richter (2015) of using the standard deviation of C_p to estimate the transition location can be effective in some cases, particularly when stationary crossflow is dominant.

As with most transition detection methods, including IR thermography, the current technique is somewhat qualitative. However, when the results are viewed in the larger context, there is often enough information available to obtain confidence in the results. It is important to keep in mind that there are other physical mechanisms that could cause a similar abrupt rise in pressure, such as a separation bubble or a shock wave. Thus, it is important to be aware of any such features that could exist. It should also be mentioned that if the pressure taps themselves trip the flow, this technique will obviously be of no use, since the pressure taps will always be under a turbulent boundary layer. Therefore, this may not be a viable technique for higher Reynolds number flows, particularly if the pressure taps begin near the leading edge.

Authors' Contributions JE came up with the idea and wrote the manuscript. JH, AL, and MK all participated in the experiment. JH performed the post-processing of the static pressure data. AL performed the post-processing of the IR transition front data. All authors reviewed the manuscript.

Funding The authors declare that they have no funding to disclose.

Data availability The data used for this study are in the process of being made available on the NASA Langley Turbulence Modeling Resource Website (Rumsey 2022).

Declarations

Conflict of interest The authors declare that they have no conflict of interes

Ethical approval This declaration is not applicable.

References

Gardner AD, Richter K (2015) Boundary layer transition determination for periodic and static flows using phase-averaged pressure data. Exp Fluids 56(6):1–13

Hall R, Carraway D, Johnson C, et al (1989) Comparisons of boundary-layer transition measurement techniques in the Langley Unitary Plan wind tunnel. In: 7th Applied Aerodynamics Conference, p 2205

Huang TT, Hannan D (1975) Pressure fluctuations in the regions of flow transition. NASA STI/Recon Tech Rep N 76(33):449

Leidy A, Kegerise MA, Hannon J, et al (2023) Measurements and computations of natural transition on the NASA juncture-flow model with a symmetric wing. In: AIAA SCITECH 2023 forum, p 0441

Liepmann H, Skinner G (1954) Shearing-stress measurements by use of a heated element. Technical Report, NACA TN, p 2368

Popov AV, Botez RM, Labib M (2008) Transition point detection from the surface pressure distribution for controller design. J Aircr 45(1):23–28

Quast AW (1987) Detection of transition by infrared image technique. In: ICIASF '87—12th International Congress on Instrumentation in Aerospace Simulation Facilities, pp 125–134

Rumsey CL (2022) NASA Langley turbulence modeling resource website. https://turbmodels.larc.nasa.gov

Rumsey CL, Ahmad NN, Carlson JR et al (2022) NASA juncture flow computational fluid dynamics validation experiment. AIAA J 60:4789–4806

Venkatachari BS, Paredes P, Choudhari MM, et al (2021) Pretest computational assessment of boundary layer transition in the NASA juncture flow model with an NACA 0015-based wing. In: AIAA AVIATION 2021 FORUM, p 2502